Chinese Journal of Aeronautics, (2014),27(6): 1598–1604

Chinese Society of Aeronautics and Astronautics
& Beihang University

Chinese Journal of Aeronautics

cja@buaa.edu.cn
www.sciencedirect.com

Calibration of robotic drilling systems with a moving rail

Tian Wei *, **Zeng Yuanfan, Zhou Wei, Liao Wenhe**

College of Mechanical and Electronical Engineering, Nanjing University of Aeronautics and Astronautics, Nanjing 210016, China

Received 8 November 2013; revised 15 January 2014; accepted 25 March 2014
Available online 18 October 2014

KEYWORDS

Aircraft assembly;
Calibration;
Error compensation;
Robotic drilling;
Robotics

Abstract Industrial robots are widely used in aircraft assembly systems such as robotic drilling systems. It is necessary to expand a robot's working range with a moving rail. A method for improving the position accuracy of an automated assembly system with an industrial robot mounted on a moving rail is proposed. A multi-station method is used to control the robot in this study. The robot only works at stations which are certain positions defined on the moving rail. The calibration of the robot system is composed by the calibration of the robot and the calibration of the stations. The calibration of the robot is based on error similarity and inverse distance weighted interpolation. The calibration of the stations is based on a magnetic strip and a magnetic sensor. Validation tests were performed in this study, which showed that the accuracy of the robot system gained significant improvement using the proposed method. The absolute position errors were reduced by about 85% to less than 0.3 mm compared with the maximum nearly 2 mm before calibration.

1. Introduction

With the maturity of robot technology in recent years, there is a broad prospect of robots applied in aerospace automated assembly for the advantages of high flexibility and automation.[1–4] For example, robotic drilling system has been applied in aerospace manufacturing for many years. Because the sizes of aircraft components are usually large, a moving rail is often used to expand the robot working range. It is necessary to improve the position accuracy of the system. However, there is a problem if the moving rail is integrated as the seventh axis in the robotic drilling system. The robot may stop at any position on the moving rail when the end effector is drilling, so the manufacturing accuracy of the moving rail must be high enough to ensure the drilling precision, which increases the cost of the moving rail and the amount of calibration work. Studying how to apply a moving rail with low accuracy into a robotic drilling system has a great value in a robot's application.

Error compensation or calibration is a common method to improve robot accuracy. Elatta et al.[5] presented an overview of robot calibration in 2004. Four sequential steps in kinematic calibration were summarized in their overview, i.e., modeling, measurement, identification, and compensation (or correction). Among the existing modeling methods including the S-model promoted by Stone and Sanderson[6] and the CPC model

* Corresponding author. Tel.: +86 25 84891836.
E-mail address: tw_nj@nuaa.edu.cn (W. Tian).

Peer review under responsibility of Editorial Committee of CJA.

ELSEVIER Production and hosting by Elsevier

http://dx.doi.org/10.1016/j.cja.2014.10.028

promoted by Zhuang et al.[7], the modified D-H model (also called MDH model) promoted by Veitschegger and Wu[8] has been used most widely. Alici and Shirinzadeh[9] described the kinematic model of a Motoman SK 120 robot using MDH convention and parameters. A laser tracker was used to measure position errors and the robot's parameter errors were identified. Nubiola and Bonev[10] proposed a 29-parameter calibration model to calibrate an ABB IRB 1600-6/1.45 robot using a laser tracker. Liu[11] enhanced robot accuracy with the maximum deviation below 0.4 mm for any axis using optimal configuration data. A CCD camera was used in the research of Motta et al.[12] to measure and identify parameter errors. Neural networks were also used by Wang and Bai[13] to improve position accuracy of robot manipulators. In their work, grid points on a standard calibration board were measured using a calibrated camera attached on a robot's end effector, and a generalized feed-forward neural network was applied to estimate position errors. Park et al.[14] employed a stationary camera and a structured laser module (SLM) attached on a robot end effector to measure the accurate position of the robot, and errors of the positions and kinematic parameters were represented via Jacobian matrices and estimated using an extended Kalman filter respectively. Zhan and Wang[15] used a hand-eye vision system to help improving robot accuracy in a robot drilling system. DeVlieg and Szallay colleagues from Electroimpact, Inc.[16,17] integrated secondary encoders to an industrial robot which yielded tighter control on axial position, and thus the robot system was compensated to high accuracies. An adaptive tracking system for industrial system (ATIR)[18] was developed in the European project COMET for real-time correction of a robot to compensate for errors during milling with the robot. The idea of ATIR was to set up a closed-loop control system with a metrological tracking system detecting the positions of the tool frame and the base frame at the same time, as well as deriving the error when comparing with the programmed path.

As can be seen from the existing literature, the majority of the researchers only focused on the calibration of the robot. However, calibration of the moving rail of a robot system was barely reported. A calibration method for both the robot and the moving rail based on multiple stations was proposed in this paper. The method was verified to be feasible by experiments.

2. Multi-station method

A long moving rail is always needed if the object of manufacture is an aircraft component. A commercial long moving rail with high precision usually costs too much. It is sometimes even more expensive than a robot. Therefore, we would have to choose using a moving rail with lower precision for economic reason, which makes the calibration of the moving rail an important issue.

The accuracy and repeatability of a customized moving rail were measured. The length of the rail was 3 m. A laser tracker was used to measure the position of a 1.5-in spherically mounted reflector (SMR) attached on the flange of a robot mounted on the rail. The six joints of the robot remained fixed during the measurement, so the errors of the moving rail were the major error sources. The position errors were measured when the slide moved in equal increments from its nominal position 0 mm to 2000 mm and then back to 0 mm. Fig. 1 shows the results of the measurement. The data along the vertical axis depict the deviations between the nominal and actual positions of the slide. It can be seen from Fig. 1 that the maximum error of the rail is already near 0.5 mm, which is critical in aircraft manufacturing. Additionally, the repeatability of the rail is not so good. The deviation between the two curves depicts the backlash of the rail (about 0.2 mm), which means the slide could not move to the same position when it is controlled by the same moving orders.

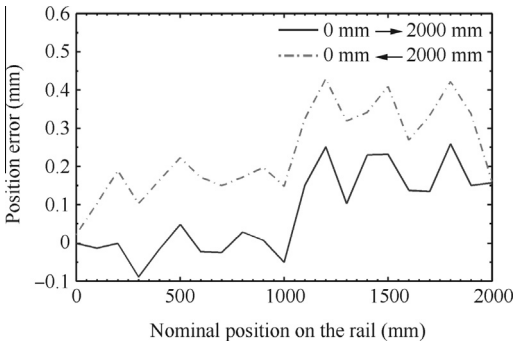

Fig. 1 Position errors of moving rail measured from 0 mm to 2000 mm and back to 0 mm.

Obviously, the precision of the robot end-effector will be influenced because of the propagation of such rail errors, so the moving rail must be calibrated before being put into service. However, the measurement for calibration is time-consuming if the moving rail is controlled as the seventh axis of the robot since the robot moves continuously on the rail. We propose a multi-station control method to control the moving rail. According to the size of the component waiting to be drilled and the working envelop of the robot, we can define several certain positions on the rail as working stations, as shown in Fig. 2. The robot just needs to stop at one station before the end-effector starts drilling. When the next drilling hole is beyond the working range of the robot, it moves to the station closest to the hole and continues drilling. If the repeatability of the rail is good enough at these stations, we

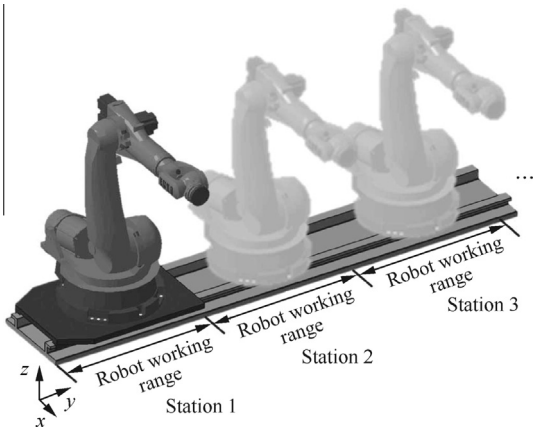

Fig. 2 Defining stations according to robot working range along moving rail.

just need to focus on the errors at these stations instead of the whole rail, which makes the calibration an easy work.

In this study, we focus on eliminating the influence on the accuracy of the robot end caused by the errors of the moving rail in a robot system. The calibration of the robot system is divided into two independent parts: the calibration of the robot and the calibration of the stations. Section 3 states the calibration of the robot based on an inverse distance weighted interpolation method. Section 4 states the calibration of the stations based on station frames. In addition, high repeatability of the moving rail is required to make sure the robot can move to a defined station precisely, so the method of improving the repeatability of the moving rail is also demonstrated in Subsection 4.3. Validation results of the calibration of the robot system are shown in Section 5.

3. Robot calibration

3.1. Error model

The error model of this study is described by Zhou et al.[19] in 2013. The mathematical representation chosen to model the kinematics of the robot is the Denavit–Hartenberg notation[20] and homogeneous transform matrices.[21] The transformation that relates the tool frame {T} to the robot's base frame {B} can be represented as

$$\boldsymbol{T}_n = \boldsymbol{A}_1\boldsymbol{A}_2\boldsymbol{A}_3\cdots\boldsymbol{A}_n \tag{1}$$

where

$$A_i = \mathrm{Rot}(z,\theta_i)\mathrm{Trans}(0,0,d_i)\mathrm{Trans}(a_i,0,0)\mathrm{Rot}(x,\alpha_i) \tag{2}$$

For a revolute joint, the joint angle θ_i is the joint variable, while the link offset d_i, the link length a_i, and the link twist α_i are fixed link parameters. According to differential kinematics, the differentiation of Eq. (2) is:

$$\mathrm{d}A_i = \frac{\partial A_i}{\partial a_i}\Delta a_i + \frac{\partial A_i}{\partial \alpha_i}\Delta\alpha_i + \frac{\partial A_i}{\partial d_i}\Delta d_i + \frac{\partial A_i}{\partial \theta_i}\Delta\theta_i = A_i\delta A_i \tag{3}$$

where $\delta\boldsymbol{A}_i$ is the error matrix of $\boldsymbol{A}_i$, i.e.,

$$\delta A_i = \begin{bmatrix} 0 & -\delta z_i^A & \delta y_i^A & \mathrm{d}x_i^A \\ \delta z_i^A & 0 & -\delta x_i^A & \mathrm{d}y_i^A \\ -\delta y_i^A & \delta x_i^A & 0 & \mathrm{d}z_i^A \\ 0 & 0 & 0 & 0 \end{bmatrix} \tag{4}$$

in which $\boldsymbol{d}^A = [\mathrm{d}x^A, \mathrm{d}y^A, \mathrm{d}z^A]^{\mathrm{T}}$ and $\boldsymbol{\delta}^A = [\delta x^A, \delta y^A, \delta z^A]^{\mathrm{T}}$ are the position and posture error vectors of frame $\{i\}$ with respect to frame $\{i-1\}$, respectively.

Now we consider the robot's forward kinematics with errors. The transformation that relates frame {T} to frame {B} may be written as

$$\begin{aligned} T_n + \mathrm{d}T_n &= (A_1 + \mathrm{d}A_1)(A_2 + \mathrm{d}A_2)\cdots(A_n + \mathrm{d}A_n) \\ &= \sum_{i=1}^{n}(A_i + \mathrm{d}A_i) \end{aligned} \tag{5}$$

If we ignore the differentials of higher order in Eq. (5), we can obtain

$$\mathrm{d}T_n = T_n\sum_{i=1}^{n}(U_{i+1}^{-1}\delta A_i U_{i+1}) = T_n\delta T_n \tag{6}$$

where $\delta\boldsymbol{T}_n$ is the error matrix of $\boldsymbol{T}_n$, and $U_i = A_iA_{i+1}\cdots A_n$. According to differential kinematics,

$$\delta T_n = \sum_{i=1}^{n}(U_{i+1}^{-1}\delta A_i U_{i+1}) = \begin{bmatrix} 0 & -\delta z^n & \delta y^n & \mathrm{d}x^n \\ \delta z^n & 0 & -\delta x^n & \mathrm{d}y^n \\ -\delta y^n & \delta x^n & 0 & \mathrm{d}z^n \\ 0 & 0 & 0 & 0 \end{bmatrix} \tag{7}$$

Finally, the position and posture error vectors of frame {T} with respect to frame {B} can be represented as $\boldsymbol{d}^n = [\mathrm{d}x^n,\ \mathrm{d}y^n,\ \mathrm{d}z^n]^T$ and $\delta^n = [\delta x^n,\ \delta y^n,\ \delta z^n]^T$.

3.2. Error similarity

We can see from the error model that the elements of the position error vector $\boldsymbol{d}^n$ are composed of the robot's link parameters and their trigonometric functions. Because only the joint angles are variables, these trigonometric functions are n-times continuously differentiable. Thus two position error vectors are similar if their corresponding joint angles are similar. Generally, the smaller the difference of the joint angles is, the more similar the error vectors are.

A concept of error similarity was proposed by Zhou et al.[19] based on the phenomenon illustrated above. The absolute position error of the robot with respect to frame {B} can be considered as a 3D vector $\boldsymbol{e}$, as shown in Fig. 3. The error similarity of error vectors $\boldsymbol{e}_1$ and $\boldsymbol{e}_2$ can be defined as:

$$\omega = \begin{cases} \infty & e_1 = e_2 \\ 1/|e_1 - e_2| & e_1 \neq e_2 \end{cases} \tag{8}$$

where ω is the error similarity.

3.3. Error compensation model based on error similarity

In this study, inverse distance weighted interpolation is used to calculate the absolute position error of the robot end. Inverse distance weighted (IDW) interpolation is a type of deterministic method for multivariate interpolation with a known scattered set of points. The assigned values to unknown points are calculated with a weighted average of the values available at the known points. The general premise of this method is that the attribute values of any given pair of points are related to each other, but their similarity is inversely related to the distance between the two locations. Analogously, the error

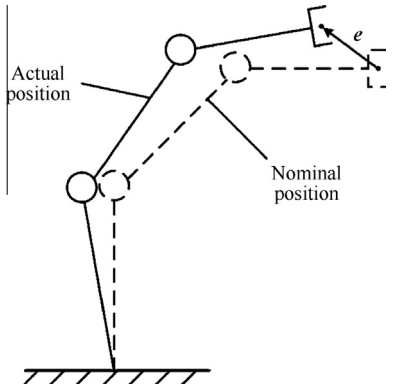

Fig. 3 Position error vector between actual and nominal positions.

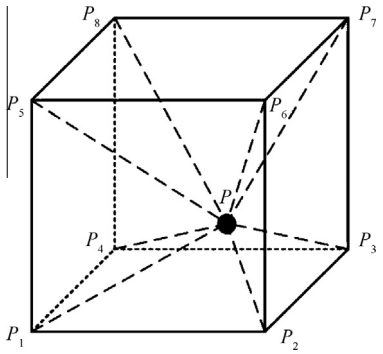

Fig. 4 IDW interpolation with eight points around point P.

similarity ω of two positions of the robot end is inversely related to their distance.

The error compensation method based on IDW interpolation is shown in Fig. 4. The error similarity between P and vertex $P_i(i = 1, 2, \ldots, 8)$ is inversely related to their distances in the cubic space. Thus the weight can be calculated as

$$q_i = \frac{\frac{1}{d_i}}{\sum_{i=1}^{8} \frac{1}{d_i}} \tag{9}$$

where q_i is the weight corresponding to vertex P_i, d_i is the distance between the nominal position of P and the actual position of P_i. Thus the absolute position error of P can be obtained by interpolating the errors of the vertexes:

$$e = \sum_{i=1}^{8} (q_i e_i) \tag{10}$$

where $\boldsymbol{e}$ is the absolute position error vector of P and $\boldsymbol{e}_i(i = 1, 2, \ldots, 8)$. is the absolute position error vector of vertex $P_i(i = 1, 2, \ldots, 8)$.

Finally, we can generate a modified robot code by adding the error e to the nominal position of P. The absolute position precision of P can be improved when the robot is driven by the modified code.

4. Stations calibration

It is a lot of work to measure the errors of the robot end at every station, so we propose a method which enables the measured data of one station to be useful to calibrate other stations.

4.1. Principle

The principle of this method is shown in Fig. 5. The absolute position errors of the robot with respect to the world frame {W} at station 1 are measured using a laser tracker. We can transform the measured data of station 1 into that of station i when the robot moves to station i, and then the transformed measured data can be used to compensate for the position errors at station i.

The transformed measured data can be represented as

$${}^{w}_{i}\boldsymbol{p}_j = {}^{w}_{i}\boldsymbol{T}\,{}^{i}\boldsymbol{p}_j \tag{11}$$

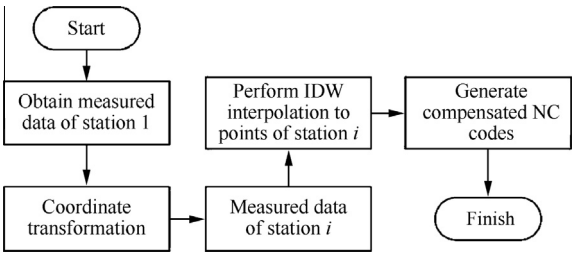

Fig. 5 Principle of stations calibration.

where ${}^{w}_{i}\boldsymbol{p}_j = [{}^{w}_{i}\boldsymbol{p}_{jx}, {}^{w}_{i}\boldsymbol{p}_{jy}, {}^{w}_{i}\boldsymbol{p}_{jz}]^{\mathrm{T}}$ is the jth measured data vector of station i with respect to frame {W}, ${}^{w}_{i}\boldsymbol{T}$ is the homogeneous transformation matrix of the robot base frame at station i, which is written as frame $\{B_i\}$, with respect to frame {W}, and ${}^{i}\boldsymbol{p}_j$ is the jth measured data vector of station i with respect to frame $\{B_i\}$.

To use the measured data of station 1, let

$${}^{i}\boldsymbol{p}_j = {}^{1}\boldsymbol{p}_j \tag{12}$$

where ${}^{1}\boldsymbol{p}_j$ represents the jth measured data vector of station 1 with respect to frame $\{B_i\}$. Then the measured data of station i can be represented by the measured data of station 1 with respect to frame {W}:

$${}^{w}_{i}\boldsymbol{p}_j = {}^{w}_{i}\boldsymbol{T}\,{}^{1}\boldsymbol{p}_j = {}^{w}_{i}\boldsymbol{T}\,{}^{1}_{w}\boldsymbol{T}\,{}^{w}\boldsymbol{p}_j = {}^{w}_{i}\boldsymbol{T}\,{}^{w}_{1}\boldsymbol{T}^{-1}\,{}^{w}_{1}\boldsymbol{p}_j \tag{13}$$

where ${}^{w}_{i}\boldsymbol{T}$ is the homogeneous transformation matrix of frame $\{B_i\}$ with respect to frame {W} and ${}^{w}_{1}\boldsymbol{p}_j$ is the measured data vector of station 1 with respect to frame {W}. Thus the position errors of the robot end with respect to frame {W} can be compensated for using the IDW interpolation at station i.

4.2. Station frame

According to the principle of this method, we should get a transformation matrix that relates frame $\{B_i\}$ to frame {W} and a transformation matrix that relates frame $\{B_i\}$ to frame {W}. Thus we should construct the robot base frame at every station using a laser tracker. Fig. 6 shows the method to get the robot's axis 1, where the 6 axis of the robot are labeled as A1, A2, ..., A6. The z-axis of the base frame is the centerline of the circle constructed by fitting several points measured when rotating the robot's axis 1. The x-axis of the base frame is the centerline of the circle constructed by fitting several points

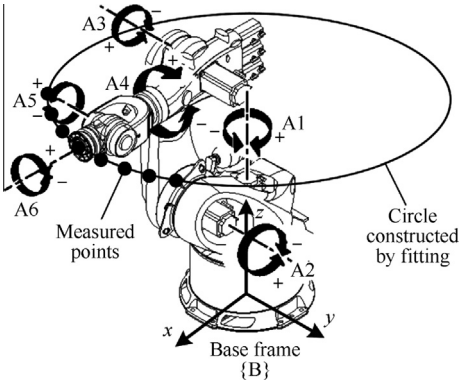

Fig. 6 Method to get robot's axis 1 using a laser tracker.

measured when rotating the robot's axis 6, using the same way as axis 1. The y-axis of the base frame is defined according to the right-hand rule.

However, the repeatability of the robot base frames is not very high, because there are inevitable errors during the measurement. Besides, the procedure to construct the robot base frame is complicated. It is a waste of time to construct every base frame at every station.

To solve this problem, we replace the robot base frame $\{B_i\}$ with a station frame $\{S_i\}$ which is constructed by measuring the positions of three arbitrary points fixed on the slide when the robot stops at station i. Fig. 7 shows the layout of the three points called P_1, P_2, and P_3 respectively. The x vector of frame $\{S_i\}$ is

$$\boldsymbol{s}_x = \frac{\boldsymbol{P}_1\boldsymbol{P}_2}{|\boldsymbol{P}_1\boldsymbol{P}_2|} \tag{14}$$

The z vector of frame $\{S_i\}$ is

$$\boldsymbol{s}_z = \frac{\boldsymbol{P}_1\boldsymbol{P}_2 \times \boldsymbol{P}_1\boldsymbol{P}_3}{|\boldsymbol{P}_1\boldsymbol{P}_2 \times \boldsymbol{P}_1\boldsymbol{P}_3|} \tag{15}$$

Thus, the y vector of frame $\{S_i\}$ is

$$\boldsymbol{s}_y = \frac{\boldsymbol{s}_z \times \boldsymbol{s}_x}{|\boldsymbol{s}_z \times \boldsymbol{s}_x|} \tag{16}$$

The repeatability of the station frame is better than that of the robot's base frame, since the positions of the three points are fixed on the slide and the construction of the station frame does not rely on fitting. In an experiment, six arbitrary points mounted on the slide were measured using a laser tracker with respect to the constructed base frames and station frames at three stations, respectively. The points measured at the stations at 300 mm and 1900 mm were compared with respect to the points measured at the station at 1100 mm, as shown in Fig. 8. The repeatability of the station frame is about 4 times better than that of the robot's base frame. In addition, the transformation that relates the station frame to the base frame is constant.

Thus the measured data of station i can be represented as:

$$\begin{aligned} {}^{w}_{i}\boldsymbol{p}_j &= {}^{w}_{i}\boldsymbol{T}\,{}^{w}_{1}\boldsymbol{T}^{-1}\,{}^{w}_{1}\boldsymbol{p}_j \\ &= \left({}^{w}_{si}\boldsymbol{T}\,{}^{si}_{i}\boldsymbol{T}\right)\left({}^{w}_{s1}\boldsymbol{T}\,{}^{s1}_{1}\boldsymbol{T}\right)^{-1}{}^{w}_{1}\boldsymbol{p}_j \\ &= {}^{w}_{si}\boldsymbol{T}\,{}^{w}_{s1}\boldsymbol{T}^{-1}{}^{w}_{1}\boldsymbol{p}_j \end{aligned} \tag{17}$$

where ${}^{w}_{si}\boldsymbol{T}$ is the homogeneous transformation matrix of frame $\{S_i\}$ with respect to frame $\{W\}$ and ${}^{si}_{i}T$ is the homogeneous transformation matrix of frame $\{B_i\}$ with respect to frame $\{S_i\}$.

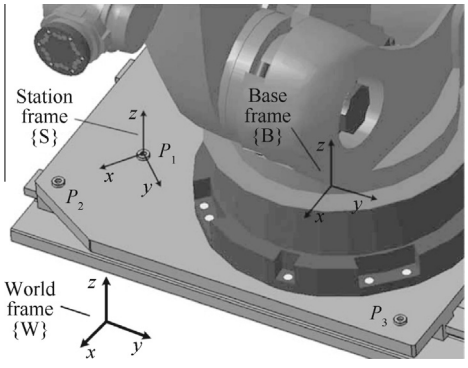

Fig. 7 Layout of station frame constructed by three points.

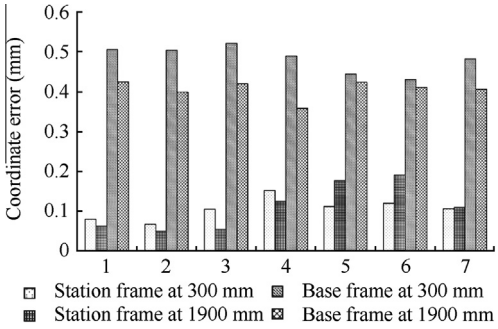

Fig. 8 Comparison of repeatability between base frame and the station frame.

4.3. Improving repeatability of rail

As discussed above, the repeatability of the moving rail is not good enough, so it is difficult for the robot to position to a defined station precisely. In order to solve this problem, we can use a linear magnetic strip and a magnetic sensor to help improving the position repeatability of the stations.

The installation of the magnetic strip and the magnetic sensor is shown in Fig. 9. The magnetic strip is used to record distance information of the stations. The resolution of the magnetic strip is 0.01 mm, which is high enough. The magnetic sensor fixed on the slide is used to measure the data gathered on the magnetic strip.

We can set up a closed-loop control system with the magnetic strip and the magnetic sensor. Firstly we move the slide to a position and define it as a station position. Then we use the magnetic sensor to record the position information on the magnetic strip. When we want the slide to move to this station again, the control system will compare the real time data gathered by the magnetic sensor with the position information recorded before and control the slide approaching to the station position. The repeatability of the stations can be ensured by this way.

An experiment was carried out to test the effectiveness of this method. The slide was controlled by the same command to move to a certain position for 15 times. The position errors were measured using a laser tracker. Fig. 10 shows that the repeatability errors of the moving rail can be compensated to less than 0.035 mm under the control of the magnetic strip and sensor.

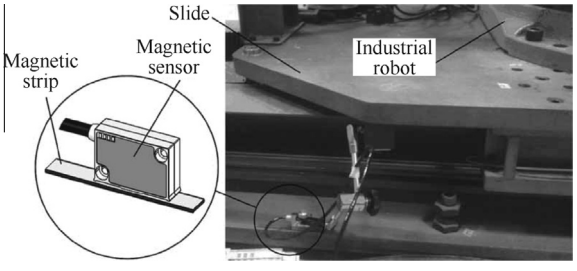

Fig. 9 Installation of magnetic strip and magnetic sensor.

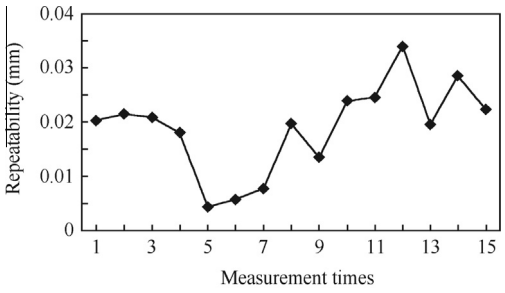

Fig. 10 Repeatability of moving rail under control of magnetic strip and magnetic sensor.

5. Experimental validation

5.1. Experimental conditions

An API T3 laser tracker was used to measure the positioning performance of a KUKA KR210 industrial robot on a moving rail. According to the specifications, the absolute distance measuring accuracy of this laser tracker within 10 m is 15 μm. The moving rail is 3 meters long and its accuracy without calibration is shown in Fig. 1.

Three positions were chosen as the stations on the moving rail to verify the proposed method. The stations were defined at 300 mm, 1100 mm, and 1900 mm. The position commands sent to the robot were Cartesian coordinate values with respect to frame {W}. The position measurements were performed with a 1.5-in spherically mounted reflector (SMR) attached on the flange of the robot. The temperatures of the laboratory were between 22 °C and 24 °C when all the measurements were performed.

Because the measuring errors rise with the increase of the measuring distance, the position of the world frame {W} was chosen in the middle of the measuring area. It was constructed in the measuring software after measuring three points which were fixed on the floor using the laser tracker.

5.2. Validation test of robot's calibration

We chose the station at 1100 mm as the station on which the robot's calibration was performed. The measuring range was 900 mm × 900 mm × 900 mm. With an increment of 300 mm, the measuring range was divided into 27 grids, as shown in Fig. 11.

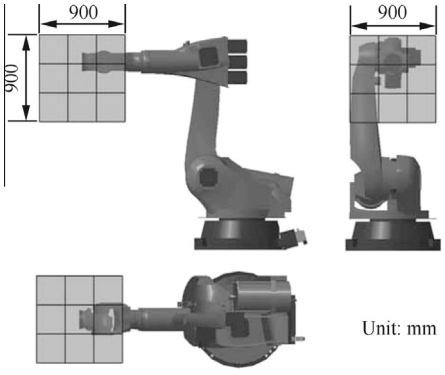

Fig. 11 Measuring range for validation test.

Firstly, the world frame {W} was measured and constructed. Secondly, the base frame {B} was measured and constructed using the method described in Section 4. Thirdly, the SMR was positioned by the robot to the vertexes of the 27 grids. Once the SMR stopped at one vertex, the laser tracker recorded its real position. Then a validation test for the IDW method was performed to 135 robot configurations randomly distributed within the measuring range. The IDW interpolation was used for each robot configuration with its nearest 8 vertexes measured before. The SMR was positioned by the robot which was controlled by the modified position codes after calibration. The absolute position errors were detected by the laser tracker as 3D errors, which were calculated according to the following equation:

$$\Delta p = \sqrt{\Delta x^2 + \Delta y^2 + \Delta z^2} \tag{18}$$

where Δx, Δy, and Δz are errors along the principal directions of frame {W}, which are the deviations between the measured coordinates and the nominal coordinates.

The test results are shown in Fig. 12. The zero positions of the robot's six joints were calibrated before the test, so the absolute position accuracy of the robot was relatively high (for high payload robots, the position error can be over 2 mm sometimes). The mean error of the robot before calibration was 1.2092 mm, while the mean error of the robot after calibration was 0.1168 mm. It can be seen from Fig. 12 that the precision of the robot was improved significantly by an order of magnitude after calibration.

5.3. Validation test of multi-station method

We chose the stations at 300 mm and 1900 mm to validate the calibration of the stations. The relationships between each station frame and the world frame were measured by the laser tracker. The measuring range of both stations was the same as that of the station at 1100 mm. The measured data of the station at 1100 mm were firstly transformed to the stations at 300 mm and 1900 mm respectively. Then the IDW interpolation method was performed to 150 robot configurations as we did for the station at 1100 mm.

The test results of both stations at 300 mm and 1900 mm are shown together in Fig. 13. The mean error of the robot before calibration was 1.2511 mm, while the mean error of the robot after calibration was 0.1600 mm, which means that the precision of the robot at other stations also got improved by an order of magnitude after calibration. The absolute position accuracy of the robot was not as good as that at the

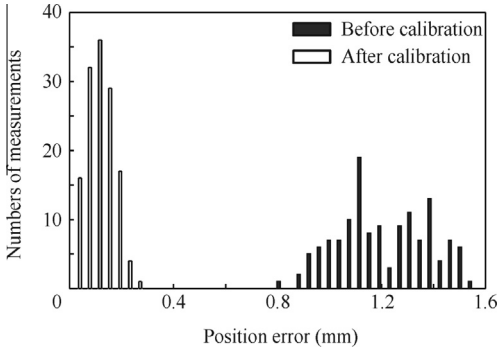

Fig. 12 Validation test results of IDW interpolation method.

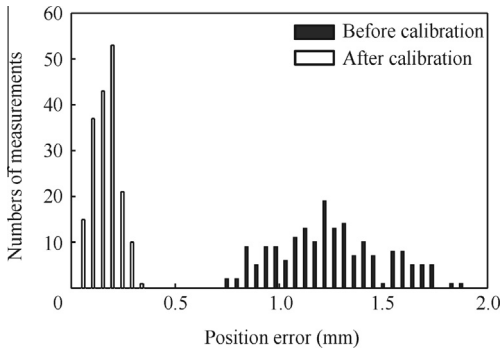

Fig. 13 Validation test results of multi-station method.

station at 1100 mm mainly because there were inevitable calculation errors in the transformations. Even so, the precision of the robot after calibration can meet the requirement of most industrial manufacture.

6. Conclusions

(1) We have demonstrated a method to compensate for the absolute position errors of a robot system with a moving rail. The method proposed in this paper is an expansion of the IDW method proposed in Ref. [19]. The IDW method is available for robots fixed on the ground or a platform, but not good enough for robots moving on a rail. The multi-station method overcomes this shortcoming.

(2) The experimental validation results showed that the IDW interpolation method based on error similarity was able to improve the absolute position accuracy of a robot effectively. The multi-station method has been proven to be valid in improving the performance of a robot on a low-accuracy moving rail.

(3) The calibration method we have proposed in this paper can meet the need of high absolute position accuracy in robot applications, especially for robot systems with a moving rail such as aircraft robotic drilling. This method makes a moving rail with low accuracy competent to do high-precision jobs, which lowers the hardware costs of the whole system in some extent. In addition, measured data of one station can be used to calibrate other stations, which saves a lot of time. The number of stations should be defined according to the size of the whole working area and the robot's moving envelop, but the distance from the world frame should not be beyond the measuring distance of the laser tracker.

Acknowledgements

This study was co-supported by the National Natural Science Foundation of China (No. 51475225) and Aeronautical Science Foundation of China (No. 2013ZE52067).

References

1. Atkinson J, Hartmann J, Jones S, Gleeson P. Robotic drilling system for 737 aileron. *Aerospace Technology Conference and Exposition*; 2007 Sep 17–20; SAE International; 2007.
2. Bi S, Liang J. Robotic drilling system for titanium structures. *Int J Adv Manuf Technol* 2011;**54**(5–8):767–74.
3. DeVlieg R, Sitton K, Feikert E, Inman J. ONCE (ONe-sided cell end effector) robotic drilling system. *SAE Automated Fastening Conference and Exhibition*; 2002 Oct 1–3; SAE International; 2002.
4. Bogue R. Europe fights back with advanced manufacturing and assembly technologies. *Assem Autom* 2012;**32**(4):312–7.
5. Elatta AY, Li PG, Fan LZ, Yu DY, Luo F. An overview of robot calibration. *Inf Technol J* 2004;**3**(1):74–8.
6. Stone HW, Sanderson AC. Statistical performance evaluation of the S-model arm signature identification technique. *Proceedings of 1988 IEEE international conference on robotics and automation*; 1988 Apr 24–29; 1988. p. 939–46.
7. Zhuang HQ, Roth ZS, Hamano F. A complete and parametrically continuous kinematic model for robot manipulators. *IEEE Trans Robotics Autom* 1992;**8**(4):451–63.
8. Veitschegger WK, Wu CH. Robot calibration and compensation. *IEEE J Robotics Autom* 1988;**4**(6):643–56.
9. Alici G, Shirinzadeh B. Laser interferometry based robot position error modelling for kinematic calibration. *Proceedings of 2003 IEEE/RSJ international conference on intelligent robots and systems (IROS 2003)*; 2003 Oct 27–31; 2003. p. 3588–93.
10. Nubiola A, Bonev IA. Absolute calibration of an ABB IRB 1600 robot using a laser tracker. *Robotics Comput Integrated Manuf* 2013;**29**(1):236–45.
11. Liu LS. Enhancing robot positioning accuracy using optimal configuration data. *J Chin Inst Ind Eng* 2005;**22**(6):443–50.
12. Motta JMST, de Carvalho GC, McMaster RS. Robot calibration using a 3D vision-based measurement system with a single camera. *Robotics Comput Integrated Manuf* 2001;**17**(6):487–97.
13. Wang DL, Bai Y. Improving position accuracy of robot manipulators using neural networks. *Proceedings of the IEEE instrumentation and measurement technology conference*; 2005 May 16–19; 2005.p. 1524–6.
14. Park IW, Lee BJ, Cho SH, Hong YD, Kim JH. Laser-based kinematic calibration of robot manipulator using differential kinematics. *IEEE/ASME Trans Mechatron* 2012;**17**(6):1059–67.
15. Zhan Q, Wang X. Hand–eye calibration and positioning for a robot drilling system. *Int J Adv Manuf Technol* 2012;**61**(5–8):691–701.
16. Devlieg R. Expanding the use of robotics in airframe assembly via accurate robot technology. *SAE Int J Aerosp* 2010;**3**(1):198–203.
17. DeVlieg R, Szallay T. Improved accuracy of unguided articulated robots. *SAE Int J Aerosp* 2010;**2**(1):40–5.
18. Lehmann C, Pellicciari M, Drust M, Gunnink J. Machining with industrial robots: the COMET project approach. In: Neto P, Moreira A, editors. *Robotics in smart manufacturing*. Berlin, Heidelberg: Springer; 2013. p. 27–36.
19. Zhou W, Liao W, Tian W. Theory and experiment of industrial robot accuracy compensation method based on spatial interpolation. *Chin J Mech Eng* 2013;**49**(3):42–8.
20. Denavit J, Harterberg RS. A kinematic notation for lower-pair mechanisms based on matrices. *Trans ASME J Appl Mech* 1955;**22**:215–21.
21. Chen ZH, Du FZ, Tang XQ. Research on uncertainty in measurement assisted alignment in aircraft assembly. *Chin J Aeronaut* 2013;**26**(6):1568–76.

Tian Wei received his B.S., M.S., and Ph.D. degrees from Nanjing University of Science and Technology in 2000, 2003, and 2006, respectively, and then became an instructor at Nanjing University of Aeronautics and Astronautics. Now he is an associate professor. His main research interests are digital flexible assembly, green remanufacturing, and so on.